A&A 369, 797–811 (2001)
DOI: 10.1051/0004-6361:20010179

Astronomy & Astrophysics

The chemical abundances in a sample of dwarf irregular galaxies

II. The case of IC 4662 and ESO 245-G05⋆

A. M. Hidalgo-Gámez[1], J. Masegosa[2], and K. Olofsson[1]

[1] Astronomiska observatoriet, Box 515, 751 20 Uppsala, Sweden
e-mail: kjell.olofsson@astro.uu.se
[2] Instituto de Astrofísica de Andalucía, CSIC, Apdo. 3004, 18080 Granada, Spain
e-mail: pepa@iaa.es

Received 29 November 2000 / Accepted 30 January 2001

Abstract. Optical spectra of H II regions of two dwarf irregular galaxies are presented. The objects are IC 4662 and ESO 245-G05. Chemical abundances were derived in all the H II regions where the forbidden oxygen line [OIII]λ4363 Å was detected. For spectra with the highest quality, a study of the spatial distribution of chemical elements in these objects were made. Generally, the chemical composition is largely constant within the H II regions studied. Some differences are found but could be attributed varying physical properties, e.g. small scale fluctuations in the temperature of the region. A comparison of the chemical abundances between different H II regions within the galaxies is made for IC 4662 and ESO 245-G05, where one of the H II regions clearly shows deviating chemical abundances.

Key words. galaxies: evolution – galaxies: irregular – galaxies: stellar content – interstellar medium: H II regions: general – galaxies: individual: IC 4662, ESO 245-G05

1. Introduction

In Paper I of this series (Hidalgo-Gámez et al. 2001; hereafter Paper I) the distribution of chemical composition in the two nearby H II regions in the dwarf irregular (dI) Local Group galaxy NGC 6822 was studied. No variations were found between the H II regions Hubble V and Hubble X, except perhaps for helium, which seems to be lower in the former region. A similar study is presented here for two additional galaxies selected from the sample of nearby dwarf irregular galaxies obtained in Hidalgo-Gámez & Olofsson (1998). The dIs chosen were IC 4662 and ESO 245-G05. The three galaxies of the study, the two presented here and NGC 6822 (Paper I), were selected on basis of their different properties in distance, environment, size and surface brightness. These properties may be crucial to our understanding of the mechanics behind the homogenization of the interstellar medium (ISM). Also, other morphological characteristics, such as the existence of a bar, may play an important role in the mixing of chemical elements (Martin & Roy 1995).

A common characteristic uniting the three galaxies is the existence of several bright H II regions which make them ideal targets for a study regarding possible variations in chemical composition. Absolute magnitudes and metallicities previously obtained are similar. However, their environments, distances and morphologies are substantially different. NGC 6822 is a small barred galaxy which belongs to the Local Group (see Paper I); IC 4662 is an isolated galaxy (Hidalgo-Gámez & Olofsson 1998) at an intermediate distance experiencing a major event of star formation (Heydari-Malayeri et al. 1990). Finally, ESO 245-G05 is a large barred galaxy in the outskirts of the Sculptor Group.

IC 4662 is a bright (μ = 21.2 mag arcsec^{-2}) galaxy in the direction of the NGC 6300 group (de Vaucouleurs 1975) at a distance of 2.50±0.02 Mpc. The most thorough study regarding chemical abundances and star formation was carried out by Heydari-Malayeri et al. (1990). These authors obtained the oxygen abundance for the brightest regions denoted A1 and A2 (hereafter; A1/A2), which dominate the galaxy in an Hα image (Heydari-Malayeri et al. 1990). Observations in the radio band (Becker et al. 1988; Harnett 1987), the infrared (Trinchieri et al. 1989; Sanders et al. 1995) and in the UV (Rosa et al. 1984) have been obtained and no peculiar characteristics were reported for this galaxy. The existence of a total of five

Send offprint requests to: A. M. Hidalgo-Gámez,
e-mail: anamaria@astro.uu.se

⋆ Based on observations made at the European Southern Observatory, La Silla, Chile.

bright H II regions, makes it a prime candidate for a study of possible inhomogeneities in the distribution of chemical elements in this object.

ESO 245-G05 (also denoted A 143) is a large ($r = 2.2 \pm .2$ kpc), low surface brightness object ($\mu = 24.0$ mag arcsec^{-2}) at $4.2 \pm .3$ Mpc, with several H II regions along the bar, evident from a continuum-subtracted Hα image (Miller 1996). This object is particularly interesting since Miller (1996) reported variations in chemical composition between H II regions within ESO 245-G05.

The main goal of this paper is to derive more information regarding the possible inhomogeneity in chemical abundances in dIs. We present data of higher signal-to-noise ratio compared to previous determinations in order to reassess whether the reported differences really do exist. In addition to new data for ESO 245-G05 we have obtained spectral information for the other three H II regions of IC 4662 (denoted B, C and D), never previously studied. A good quality spectrum was obtained for region A1/A2 which allows a two-dimensional mapping of this region similar to the one carried out for Hubble V and Hubble X in NGC 6822. The distribution of the elemental abundances as well as the extinction, excitation and ionization are studied in regions of 22 pc. The quality of the spectra of ESO 245-G05 allows detection of the weak emission line [OIII]λ4363 Å in two of the regions observed.

In the next section the acquisition of the data is described and the analysis is discussed in Sect. 3. Section 4 is devoted to the extinction determination and in Sect. 5 the chemical abundances of the H II regions in the sample are presented. The spatial distribution throughout the regions A1/A2 in IC 4662 is studied in Sect. 6 and a discussion of possible inhomogeneities of chemical elements is presented in Sect. 7. Conclusions are given in Sect. 8.

2. Observations

Spectra were obtained with the use of the ESO (European Southern Observatory) 3.6 m telescope at La Silla, Chile, on the 8th and 9th of August 1997. EFOSC1 was used to obtain spectra as well as Hα- and continuum images. These images were used as an aid for positioning the slit. The characteristics of the CCD detector were described in Paper I. Three grisms were used for the observations. Nr. 6 and nr. 10 in the ESO list of grisms have a resolution of 8 Å and cover a range in wavelength between 3720–5530 Å and 5150–6900 Å. Spectra obtained through these grisms were used in the analysis. For the purpose of obtaining an accurate extinction determination (see Sect. 4) a ten minute exposure was obtained through grism nr. 2 for each telescope position. This grism encompassed the spectral range from 3720 Å to 6750 Å. Further details regarding the grisms and the slits used during the observations are described in Paper I.

Two different slit positions were used for each galaxy. Table 1 presents the individual H II regions, the coordinates, position angles, total integration times for the blue and the red spectral regions, as well as the air mass for each position. Due to poor weather conditions, only data for the blue spectral region is presented for ESO 245-G05 nr. 19. Two subexposures were taken at each position in order to check for cosmic events. The sky was clear at the zenith position except during the end of the first night. The seeing conditions were stable during the observations, with values smaller than 1.″2 for all the positions except that for ESO 245-G05 nr. 19 where the seeing was 1.″4. Air masses during the observations of ESO 245-G05 were quite small and no correction for differential refraction was made. In the case of IC 4662 the air masses were higher and, using Table 2 of Fillipenko (1982), a correction was made.

The initial slit position for IC 4662 passed in the SE-NW direction through the main body of the galaxy, where the two H II regions, A1/A2, (Heydari-Malayeri et al. 1990), were located. The second slit was positioned in the SSE-NNW direction through the three bright H II regions, B, C and D, located to the southeast of the main body. The oxygen emission line [OIII]λ4363 Å was detected in regions A1/A2 and D only. The latter is the most distant region to the main body.

A slit was positioned along the bar in ESO 245-G05, encompassing four of the H II regions (Miller 1996). A second slit was positioned in the EW direction parallel to the first one but slightly towards the north in order to fully encompass all the regions in the southern part of the bar. A third slit was positioned to pass through the northeast extreme of the bar and the adjacent regions (nr. 1 to 10 in Miller 1996). Due to the poor signal-to-noise ratio in the emission line [OIII]λ4363 Å, only two out of eight regions were finally studied (nr. 19 and nr. 12 in Miller 1996).

The reduction was performed with the software package MIDAS. Bias and flat-fielding were performed with bias-frames and continuum lamps. He-Ar arcs were used for the wavelength calibrations. The flux calibrations were performed using spectra of the standard stars LTT 1788 and LTT 1020, with an accuracy of 5% and 8% in the blue and red spectral regions, respectively. The tables of La Silla were used for the atmospheric extinction correction. See Paper I for a more detailed description regarding the reduction process.

3. The analysis of data

A study of the spatial distribution in the chemical abundances within the H II regions was made for the high quality spectra of IC 4662 A1/A2. For these regions the two-dimensional spectra were divided, as described in Paper I, into three-row spectra (hereafter; 3r-spectra). At the distance of this galaxy, a 3r-spectrum comprises a physical region of 22 pc. The total number of spectra for the H II regions of IC 4662 are 20 for region A1 and 32 for region A2. The same procedure for region D resulted in 27 spectra. These numbers correspond to total sizes of 448 pc, 717 pc and 330 pc, respectively. As a consequence of the low signal-to-noise ratio, no further analysis was carried out for region D. These numbers are based on

Table 1. The log of the observations. The H II regions observed are presented in Col. 1. Column 2 gives the date of the observations while Cols. 3 and 4 present the telescope coordinates. The position angle is given in Col. 5. The total integration time is given in Col. 6 and the air mass in Col. 7

H II region	Date	α	δ	Pos. Angle degrees	Int. Time blue/red	Air Mas. blue/red
IC 4661 A1/A2	080897	$17^h46^m59^s$	$-64°38'43''$	289	$30^m/20^m$	1.24/1.23
IC 4661 D	090897	$17^h46^m50^s$	$-64°39'02''$	310	$60^m/100^m$	1.26/1.36
ESO 245-G05 nr. 19	080897	$01^h45^m01^s$	$-43°37'20''$	270	40^m	
ESO 245-G05 nr. 12	090897	$01^h45^m05^s$	$-43°37'21''$	295	$90^m/60^m$	1.08/1.04

different emission lines, mainly [OII]λ3727 Å in the blue and Hα in the red spectral regions. The alignment of both the blue and the red spectral regions was carried out with the aid of the continuum emission between 5200 Å and 5400 Å, which is the spectral region where the blue and the red overlap. The overlap is perfect for IC 4662 A1 but a displacement of a few pixels was found for IC 4662 A2. The same problem prevail for ESO 245-G05 nr. 12.

To gain insight into the possible existence of variations in the chemical abundance between H II regions in dI galaxies, spectra with high signal-to-noise ratios are desirable. Therefore, all the rows where the [OIII]λ4363 Å line was detected were summarized, which resulted in a one-dimensional spectrum for each H II region. The number of rows where [OIII]λ4363 Å was detected was: 10 for IC 4662 A1, 11 for IC 4662 A2, 6 for IC 4662 D, 9 for ESO 245-GO5 nr. 19 and 16 for ESO 245-G05 nr. 12, corresponding to 6.1, 6.7, 3.7, 5.7 and 9.8 arcsec, respectively.

The intensities of the spectral lines were measured with software developed at Uppsala Astronomical Observatory. Consult Paper I for more details regarding the analysis. The spectral resolution of the configuration (8 Å nominal but 16 Å considering the seeing conditions) was not sufficiently high to resolve the doublet [SII]$\lambda\lambda$6717,6731 Å. In this case, a special routine in the software, described in Paper I, was used for handling blended lines.

A set of intensities for each 3r and spatially-averaged spectrum was obtained. Spectra with a perfect alignment were normalized to the intensity of the Hβ line. In the case of small displacements, the lines in the blue part of the spectrum were normalized to the intensity of the Hβ line. Correspondingly, lines in the red were normalized to the intensity of the Hα line.

The one-dimensional spatially-averaged spectra are shown in Fig. 1 (IC 4662) and Fig. 2 (ESO 245-G05).

3.1. Errors in the continuum and line intensities

As discussed in Paper I, three different sources of uncertainty have been considered for the intensity of the spectral lines: uncertainties introduced by the reduction process, uncertainties due to the extinction corrections and uncertainties in the level of the spectral continuum, with respect to the line.

The latter was found to be the major contributor. Typical values of the uncertainty introduced by the extinction correction were only 30% of the uncertainties in the continuum. The corresponding values due to the flux calibrations are 5% in the blue and 8% in the red spectral region.

Two more terms were added for some lines. In the case of blended lines, an additional term was added which takes into account the goodness of the deblending procedure. The uncertainties are 11% for [SII]$\lambda\lambda$6717,6731 Å, 15% for [NII]λ6548-Hα and 18% for [OI]λ6300-[SIII]λ6312 Å for IC 4662 A1/A2. The corresponding values for IC 4662 D were 22%, 30% and 59%.

For IC 4662 a correction term, corresponding to the differential refraction, was added to spectral lines affected. It was found that a correction of 15% was necessary for the line [OII]λ3727 Å. No other lines were affected by differential refraction.

A total uncertainty was obtained adding together all the terms considered for each line. These are shown in Table 2 for the 3r-spectra of IC 4662. These values correspond to spectra with the lowest signal-to-noise ratios in the emission line [OIII]λ4363 Å and should therefore be considered as the maximum statistical errors.

4. The correction for underlying absorption and extinction

4.1. Underlying stellar absorption correction

All the intensities of the lines in the red spectral range, except those of IC 4662 A1/A2, were normalized to the Hα intensity. Subsequently, a correction for the underlying stellar absorption in the Balmer lines was performed (consult Paper I for details). The equivalent width of the absorption feature in the Balmer line Hβ was found to be 3 Å, for the H II regions in ESO 245-G05. This feature was not measurable in spectra of IC 4662.

4.2. The extinction correction

A correction for the extinction due to possible intergalactic and interstellar dust was applied. It should be emphasized that, in this investigation, the total amount of extinction was considered and no distinction was made between the contribution of various sources of extinction.

The extinction correction, applied to both sets of data (the 3r and the spatially-averaged spectra), was performed using the Balmer decrement with the Whitford modified extinction law (Savage & Mathis 1979).

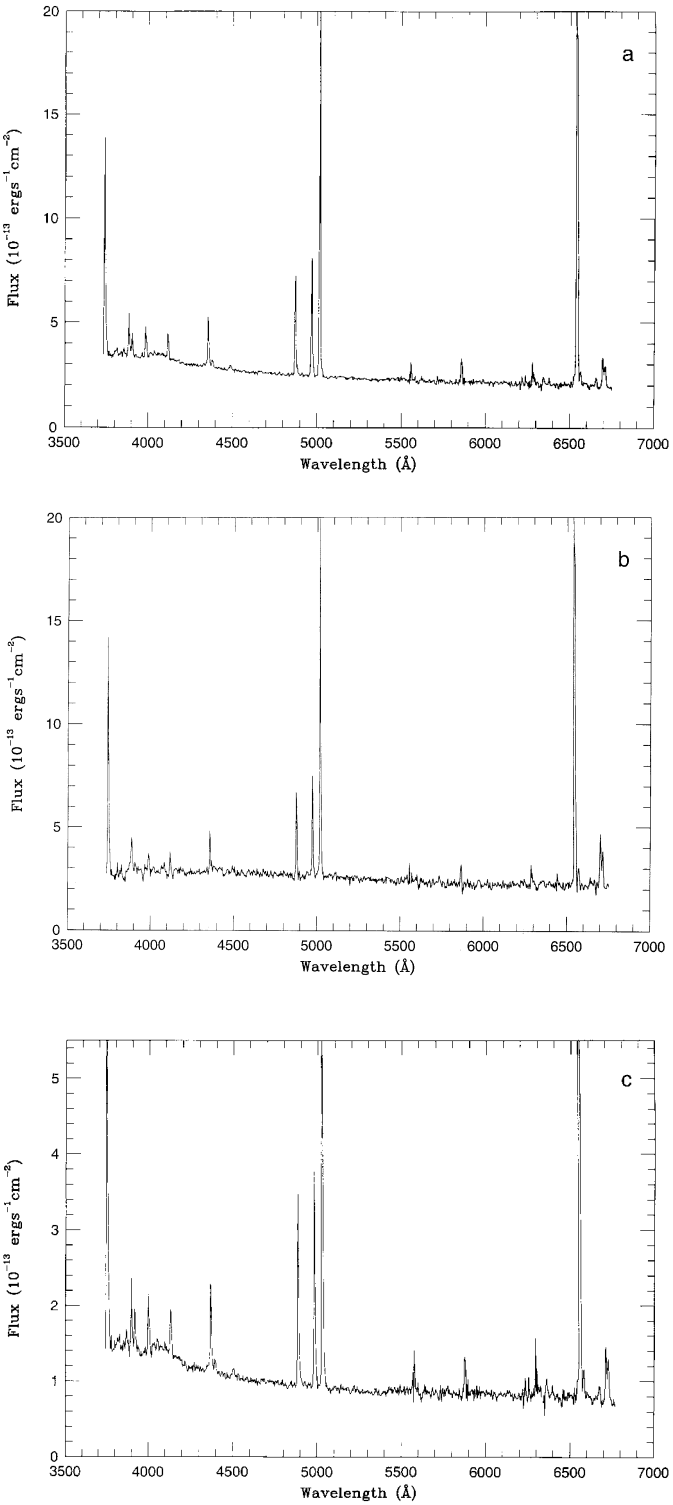

Fig. 1. The spatially-averaged spectrum of **a)** IC 4662 A1, **b)** IC 4662 A2 and **c)** IC 4662 D

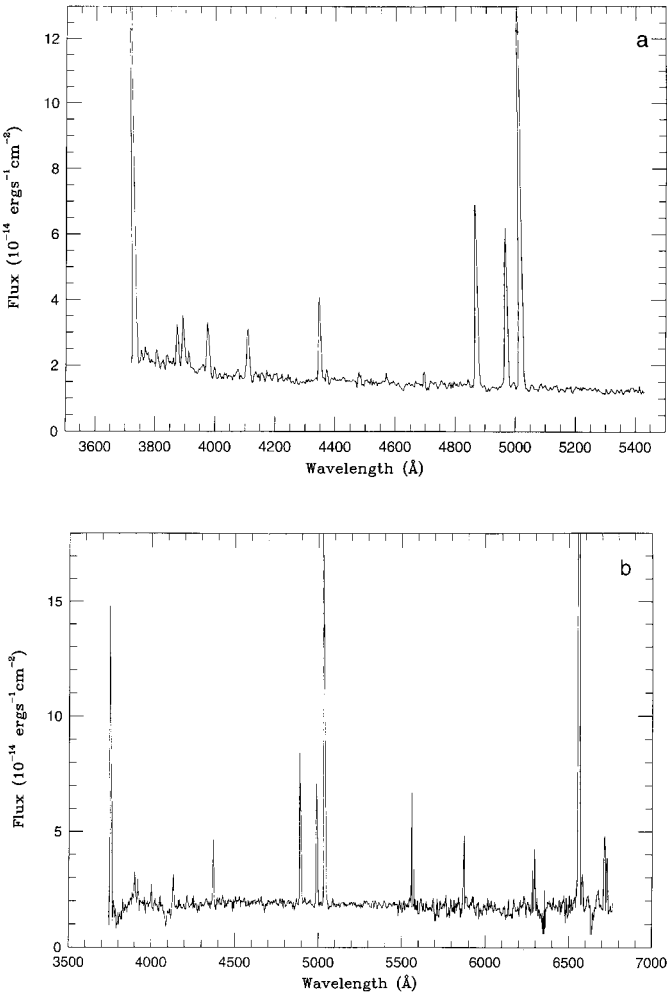

Fig. 2. The spatially-averaged spectrum of **a)** ESO 245-G05 nr. 19, **b)** ESO 245-G05 nr. 12

For spectra where the overlap between the blue and red spectral regions was not ideal, the Balmer line Hγ was used in the determination of the extinction coefficient, instead of Hα. It is well known that the Hγ line suffers a higher amount of stellar absorption than does the Hα line. In order to determine whether the extinction performed here is reasonable, a new extinction coefficient was determined using a spectrum observed with grism nr. 2 which allowed the entire spectral region to be observed, including the Hα and Hβ lines. No significant differences in the intensities of the spectral lines were found. This will be discussed in more detail in Sect. 5. The H II region ESO 245-G05 nr. 12 was found to be practically free of dust.

Table 3 presents the extinction coefficients, C_β, for the H II regions studied in this investigation, all determined from the spatially-averaged spectra. In the case of IC 4662 A1/A2, several Balmer lines were observed and a C_β was obtained for each of the lines. Only the Hγ and Hδ lines were detectable in IC 4662 D, and only the Hγ line in ESO 245-G05 nr. 19 and nr. 12. The extinction coefficients tend to increase toward shorter wavelengths, indicating an increasing importance of underlying stellar absorption. Table 3 also presents the colour excess determined from the data obtained in this investigation, the extinction coefficients available in the literature for these regions, and the colour excess from the RC3 catalogue (de Vaucouleurs et al. 1992). It should be pointed out that these last values correspond to the whole galaxy, while the $E(B-V)$ determined in this analysis are the values for the H II regions.

Table 2. The maximum uncertainties in the intensity of the emission lines. These values correspond to the 3r-spectra with the lowest signal-to-noise ratios in the line [OIII]λ4363 Å and reflect the quality of spectra

Line	IC 4662 A1	IC 4662 A2	IC 4662 D
[OII]λ3727	18	60	43
[NeIII]λ3869	24	60	68
HeIλ3889	0	0	26
[NeIII]λ3967	59	62	25
Hδ λ4102	0	0	68
Hγ λ4340	0	0	34
[OIII]λ4363	83	51	88
HeIλ4471	97	37	61
Hβ λ4861	0	0	43
[OIII]λ4959	11	7	65
[OIII]λ5007	11	7	45
HeIλ5875	21	26	62
[OI]λ6300	0	0	90
[SIII]λ6312	0	0	90
[OI]λ6363	0	-	93
[NII]λ6548	44	94	94
Hα λ6563	0	0	51
[NII]λ6583	26	34	51
HeIλ6678	78	59	55
[SII]λ6716	49	64	76
[SII]λ6730	48	69	72

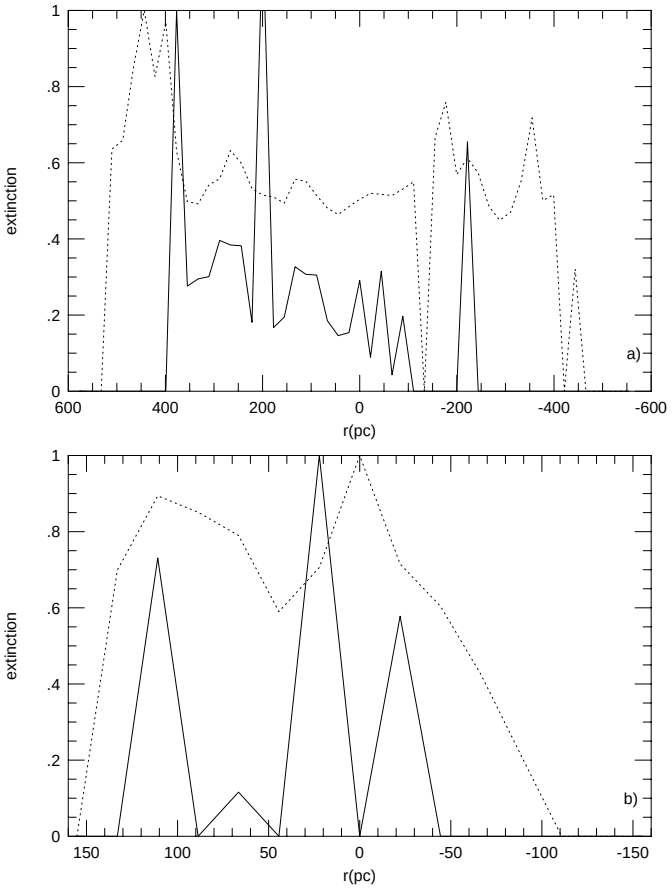

Fig. 3. The extinction across the face of the H II regions **a)** IC 4662 A1/A2 and **b)** IC 4662 D. The extinction coefficient, C_β (——), based on the Hγ line, is shown, as well as the non reddening-corrected Hα/Hβ emission line ratio ($\cdots$). The high peaks at the edges are probably an effect of the poor signal-to-noise ratio in the outer parts of the H II regions. Positive distances correspond to the southeast direction

4.3. The extinction within the H II regions of IC 4662

Because of the large size of the H II regions, as well as the high signal-to-noise ratio of some of the spectral lines, a study of the extinction over the face of these regions was possible. The extinction coefficients obtained from the 3r-spectra are presented in Fig. 3 as a function of the distance from the geometrical center at zero pc. The distance was obtained from the total emission region in Hα for A1/A2 and also from the [OII]λ3727 Å emission region for D. These are the most spatially extended lines in each spectrum.

As pointed out by González-Delgado et al. (1994), a correlation between the Hα line intensity and the C_β suggests a mixing of the ionized gas with the dust. The Hα/Hβ line ratio, not corrected for reddening, is also shown in Fig. 3. C_β determined from the Hα/Hβ line ratio mimics the behaviour of the Hα line independent of the origin of the extinction. Therefore, the C_β determined from the Hγ/Hβ line ratio is preferred for all regions, A1/A2 and D.

The behaviour of these two parameters is not exactly the same over the face of the objects. The intensity of Hα is constant in regions A1/A2, while the C_β, obtained from both the Hα and Hγ intensities, gives smaller values toward the northwestern part of the object. The "bumps" observed in both Hα and C_β, at 250 pc, 100 pc, and 175 pc may be indicative of a clumpy origin of the dust. The Hα line intensity and the C_β seem more correlated in region D. This indicates a high amount of internal dust. Due to small number statistics, these results should be treated with caution.

5. The spatially-averaged chemical abundances

As previously mentioned, a spectrum for each H II region was obtained, adding all the pixels where the emission line [OIII]λ4363 Å was detected. The total number of pixels correspond to total sizes of 224 pc for A1, 246 pc for A2 and 134 pc for D of IC 4662, 113 pc for nr. 19 and 201 pc for nr. 12 of ESO 245-G05. The emission line intensities, corrected for extinction and underlying stellar absorption including the uncertainties, are presented in Table 5. Also, the equivalent width, the flux in the Hβ emission line, as well as the signal-to-noise ratio in the [OIII]λ4363 Å line, are tabulated.

In order to derive the ionic chemical abundances, a five-level, two-zone model was used. The abundances are determined with the use of the temperature-sensitive method (Osterbrock 1989). For more details regarding the model and the derivation of the abundances see Sect. 5.1 in Paper I.

Table 3. The extinction coefficients, C_β, derived from the non-corrected Balmer line intensities. The coefficients reported in the literature are marked $C_{\beta\rm lit}$. The color excess obtained with the C_β derived in this analysis and the values compiled from the RC3 catalogue (de Vaucouleurs et al. 1991) are also presented. It should be noted that the latter values correspond to the whole galaxy. References: (1) Heydari-Malayeri et al. 1990; (2) Miller 1996

line	IC 4662 A1	IC 4662 A2	IC 4662 D	ESO 245-05 nr. 19	ESO 245-05 nr. 12
H12	-	7 ± 2	-	-	-
H10	$6.38 \pm .01$	6.4 ± 1	-	-	-
H9	$5.9 \pm .5$	6 ± 1	-	-	-
Hδ	$1.42 \pm .01$	$1.419 \pm .001$	0.073	-	-
Hγ	$2.345 \pm .004$	$1.14 \pm .02$	0.23 ± 0.03	$1.35\pm$	0.03 ± 0.02
Hα	$0.16\pm.06$	$0.20\pm.04$	-	-	-
E(B-V)	0.11	0.14	0.16	0.95	0.02
$C_{\beta\rm lit}$	0.13 (1)	0.13 (1)	-	0.35 (2)	0.70 (2)
$E(B-V)_{\rm RC3}$	0.34	0.34	0.34	0.44	0.44

Table 4. The extinction coefficient, the equivalent width of the $H\beta$ emission line, $E_v(H\beta)$ (in Å), the flux in the $H\beta$ line (in erg s^{-1}cm^{-2}) as well as elemental abundances from previous investigations. The regions are: IC 4662 A1 (first column) and IC 4662 A2 (second column) of Heydari-Malayeri et al. (1990). ESO 245-G05 nr. 12, (third column) and ESO 245-G05 nr. 19 (fourth column) of Miller (1996)

	1	2	3	4
C_β	0.13	0.13	0.35	0.7
$E_v(H\beta)$	146	122	206	70
$\log F(H\beta)$	-12.37	-12.41	-14.1	-14.37
$T_{\rm e}({\rm O}^{++})$	-	-	12100	-
12+log(O/H)	8.11	8.04	7.90	8.20
$N({\rm He})/N({\rm H})$	0.101	0.099	-	-
12+log(Ne/H)	7.35	7.35	-	-

The atomic chemical abundances were obtained from the ionic ones and the ionization correction factors (ICF) for nitrogen and neon. No ICF for oxygen is necessary since all the important ionization stages are within the wavelength range studied. No ICF was used for helium, following Izotov et al. (1999). Except for ESO 245-G05 nr. 19, where only the blue spectral region was available, the helium abundances were determined using a weighted average value of the three lines, HeIλ4471 Å, HeIλ5875 Å and HeIλ6671 Å, which are less affected by collisional excitation (Izotov et al. 1997). These atomic abundances are presented in Table 6.

The helium, nitrogen, oxygen and neon abundances, as well as their ICF, when determined, are tabulated. The log(N/O) and log(Ne/O) are also compiled, as well as the electron temperature, $T_{\rm e}$, and the temperature of the ionizing radiation, $T_{\rm ion}$. From viewing Table 6 it can be concluded that there are some variations in the abundances of helium, nitrogen, oxygen and/or neon.

5.1. Comparison with previous results

Two previous investigations of the same objects were selected for comparison with the data presented in this analysis. The data are presented in Table 4.

5.1.1. IC 4662

Heydari-Malayeri et al. (1990) obtained angular sizes of A1/A2 of 5″ and 4.″5, respectively. The sizes obtained in this analysis, which is based on the extent of the objects in the two-dimensional spectrum, are three and a half and four times larger for regions A1/A2, respectively. This corresponds to 17.″7 and 18.″3, considering the number of pixels occupied by the emission in the Hα line and the pixel size of the instrumentation. These observations were performed in the SE-NW direction, as mentioned previously, and due to the non-sphericity of the H II regions, the discrepancy could be due to a projection effect. No information on the position of the spectroscopic slit was given in Heydari-Malayeri et al. Similar abundances of helium, oxygen and neon are obtained in both investigations. This concerns also the flux in the Hβ emission line. No spectroscopic results were presented for region D in Heydari-Malayeri et al. (1990).

5.1.2. ESO 245-G05

This object was studied by Miller (1996). The chemical abundances presented by Miller were derived with the use of the so-called semi-empirical method (e.g. McGaugh 1994). Despite the different approaches taken, the results reached by Miller (1996) are close to those obtained in this analysis (see Sect. 5.3) Moreover, comparable values of the flux in Hβ are obtained in both investigations. One should note that Miller (1996) derived a smaller amount of extinction than derived in the present investigation. As evident from Table 3, a high extinction agrees with the color excess found for this galaxy.

5.2. Spectral characteristics and chemical abundances of IC 4662 A1/A2

As a consequence of the high signal-to-noise ratio of spectra of A1/A2, many lines are clearly detected. Comparing the columns corresponding to IC 4662 A1 and IC 4662 A2, both H II regions have almost identical intensities of the lines, as well as the equivalent width and flux in the Hβ

Table 5. Line intensities of the spatially-averaged spectra, normalized to the Hβ emission line, of the H II regions studied in this investigation. The equivalent width and the flux in the Hβ line (given in units of erg s^{-1}cm^{-2}), as well as the signal-to-noise ratio in the line [OIII]λ4363 Å, denoted by σ(l), are also presented

line	λ (Å)	IC 4662 A1	IC 4662 A2	IC 4662 D	ESO 245-G05 19	ESO 245-G05 12
[OII]	3727	1.1 ± .2	1.1 ± .2	2.31 ± .03	2.9 ± .2	2.5 ± .1
H12	3750		.006 ± .01			
H10	3798	0.017 ± .003	.017 ± .005			
HeI	3820	0.02 ± .01	0.02 ± .01			
H9	3835	0.03 ± .01	0.03 ± .02			
[NeIII]	3869	0.40 ± .06	0.40 ± .02	0.3 ± .1	0.27 ± .01	0.27 ± .01
HeI	3889	0.15 ± .03	0.14 ± .04	0.18 ± .04	0.27 ± .01	0.149 ± .004
CaII	3934	0.010 ± .01	0.008 ± .005			
[NeIII]	3967	0.21 ± .03	0.21 ± .03	0.36 ± .02	0.3 ± .1	0.20 ± .03
HeI	4026	0.013 ± .002	0.014 ± .002			
[SII]	4068	0.006 ± .004	0.01 ± .02			
	+4076					
Hδ	4102	0.20 ± .01	0.204 ± .001	0.20 ± .01		0.21 ± .01
Hγ	4340	0.35 ± .01	0.41 ± .01	0.47 ± .1	0.47 ± .01	0.5 ± .1
[OIII]	4363	0.07 ± .01	0.07 ± .02	0.09 ± .01	0.046 ± .005	0.09 ± .01
HeI	4471	0.04 ± .01	0.04 ± .01	0.10 ± .02	0.08 ± .01	0.038 ± .003
[FeII]	4570	0.007 ± .002	0.008 ± .005			
HeII	4650	0.04 ± .01	.04 ± .02			
ArIV]	4711	0.016 ± .001	0.015 ± .001			
ArIV]	4740	0.007 ± .001	0.007 ± .002			
Hβ	4861	1.00 ± .02	1.00 ± .02	1.00 ± .01	1.00 ± .1	1.00 ± .1
HeI	4921	0.008 ± .002	0.008 ± .001			
[OIII]	4959	2.1 ± .1	2.1 ± .1	1.1 ± .1	0.82 ± .02	0.93 ± .04
[OIII]	5007	6.4 ± .2	6.3 ± .2	3 ± 1	2.4 ± .1	2.8 ± .1
[ClIII]	5517	0.005 ± .005	0.012 ± .004			
[ClIII]	5530	0.005 ± .001	0.011 ± .004			
HeI	5875	0.11 ± .01	0.11 ± .01	0.13 ± .03		0.12 ± .01
[OI]	6300	0.004 ± 0.003	0.005 ± .001	0.09 ± .02		0.023 ± .001
[SIII]	6312	.02 ± .01	0.03 ± .01	0.04 ± .01		0.010 ± .002
[OI]	6363	0.004 ± .001	0.004 ± .002	0.04 ± .01		0.010 ± .001
[NII]	6548	0.02 ± .01	0.02 ± .01	0.03 ± .01		0.023 ± .001
Hα	6563	2.86 ± .30	2.86 ± .20	2.79 ± .06		2.86 ± .10
[NII]	6583	0.05 ± .01	0.05 ± .01	0.07 ± .01		0.15 ± .01
HeI	6678	0.03 ± .01	0.03 ± .01	0.04 ± .01		0.043 ± .004
[SII]	6716	0.10 ± .05	0.09 ± .04	0.2 ± .1		0.3 ± .1
[SII]	6730	0.06 ± .03	0.06 ± .03	0.1 ± .1		0.2 ± .1
E_v(Hβ) Å		91	91	46	193	181
log F(Hβ)		−12.14	−12.17	−12.45	−13.17	−13.06
σ(l)$_{\lambda 4363}$		19	19	6.4	2.5	3.9

Table 6. The spatially-averaged parameters derived for the H II regions in IC 4662 and ESO 245-G05. The bottom row refers to a determination of the oxygen abundance with the use of the semi-empirical method (McGaugh 1994)

line	IC 4662 A1	IC 4662 A2	IC 4662 D	ESO 245-G05 nr. 19	ESO 245-G05 nr. 12
$T_e(O^{++})$	12 000 ± 500 K	12 000 ± 1000 K	17 700 ± 400 K	14 800 ± 500 K	19 200 ± 750 K
T_{ion}	44 000 ± 4000 K	44 000 ± 3000 K	47 000 ± 5000 K	-	49 000 ± 3000 K
12+log(O/H)	8.17 ± .03	8.17 ± .05	7.7 ± .1	7.80 ± .01	7.59 ± .02
ICF(N)	7.8 ± .2	8 ± 1	2.3 ± .9	-	2.1 ± .2
12+log(N/H)	6.78 ± .07	6.66 ± .07	6.1 ± .3	-	6.32 ± .05
log(N/O)	−1.50 ± .04	−1.51 ± .02	−1.58 ± .01	-	−1.27 ± .01
ICF(Ne)	1.15 ± .01	1.15 ± .02	1.8 ± .9	2.11 ± .03	1.9 ± .1
12+log(Ne/H)	7.34 ± .02	7.35 ± .02	7.2 ± .3	7.28 ± .01	7.08 ± .03
log (Ne/O)	−0.83 ± .01	−0.83 ± .03	−0.5 ± .1	−0.52 ± .01	−0.52 ± .01
N(He)/N(H)	0.109 ± .004	0.11 ± .04	0.17 ± .03	-	0.13 ± .01
12+log(O/H)$_{sem}$	8.1	8.1	8	8.0	8.0

emission line. The main reason could be that they are physically connected, which is supported by the Hα image. On the other hand, Heydari-Malayeri et al. (1990), obtained Hβ images of the same regions and claimed that the two regions were clearly distinct. In order to compare the results from this investigation with that of Heydari-Malayeri et al. (1990), two H II regions will be considered: A1 to the northwest and A2 to the southeast.

Comparing the emission line ratios derived in this investigation with those from models of photoionization by hot stars (Stasińska 1990), it is evident that any substantial contribution from shock-heating or non-thermal radiation can be ruled out.

The detection of the doublet [ClIII]$\lambda\lambda$5517,5537 Å can be explained by photoionization only (Stasińska 1990). The ionic abundance of chlorine can be derived for A1/A2 in the same manner as for Hubble V and X in NGC 6822 (Paper I). Values of $N(Cl^{++})/N(H^+) = 2.0\ 10^{-8}$ and $4.8\ 10^{-8}$ were obtained for A1/A2, respectively. These are lower than that of Hubble X but higher than the ionic abundance of chlorine derived for Hubble V. The ratio $\log(Cl^{++}/O^{++})$ was determined for regions A1/A2 and were found to be -3.8 and -3.4, respectively, which are also intermediate between those of Hubble V and Hubble X.

One can also note the presence of the absorption line CaIIλ3934 Å (as well as CaIIλ3968 Å although blended with Hϵ) in the spectrum of IC 4662 A1/A2. This indicates the presence of an older stellar population underlying the H II region. This in turn emphasizes the importance of correcting for underlying absorption in order to obtain the chemical abundances of the nebular component.

Finally, the line HeIIλ4686 Å was detected at various positions along IC 4662 A1/A2. The origin of this line can be nebular, indicating a very hot stellar population, but can also be due to WR stars (Aller 1984). In the latter case one would expect the presence of the broad spectral feature around λ4650 Å, and also another broad feature in the spectral region between 5700–5800 Å, often referred to as the red bump. In A1/A2, in both the spatially-averaged spectra, as well as the 3r-spectra, the equivalent width of the HeII line is small, 3 Å for the spatially-averaged spectrum of A1. The absence of the WR feature in the red spectral region, in combination with the narrowness of the HeII line, the WR origin for this line can be ruled out. Instead, a nebular origin is proposed. The presence of the nebular lines [ArIV]$\lambda\lambda$4711,4740 Å supports the nebular origin. The detection of the lines over a large portion of the H II region, about 245 pc, also favours the nebular origin. Even though the spectral characteristics point to a nebular origin, the temperature of the ionizing radiation does not. For both regions the metallicity as well as the $T_{\rm ion}$ is very similar, 43 700 K and 44 700 K, respectively. The $T_{\rm ion}$ is determined from a single-burst model of spectral evolution (Olofsson 1997), These temperatures are too low to ionize helium twice, which in turn excludes a nebular origin. The situation is obviously somewhat confusing.

5.2.1. The interesting case of IC 4662 D

As evident from Table 6, the chemical abundances derived for IC 4662 D are substantially different from those of regions A1/A2. The largest deviations concern the nitrogen and oxygen abundances, 0.6 and 0.5 dex, respectively. The abundance of neon is similar, within the uncertainties. The difference in the abundances between regions A1/A2 and D cannot be explained only by uncertainties in the measurements.

One possible explanation for these differences could be the extinction correction. As mentioned in Sect. 4.2, the intensities of the lines of IC 4662 D were corrected using the Hγ line instead of the Hα line. In order to determine if the correction performed is erroneous, the following approach was taken. A new set of extinction corrected intensities were obtained with the C_β value from spectra obtained with grism nr. 2 (see Sect. 2). The result is that, despite the fact that the extinction coefficients are very different, the resulting oxygen abundances are the same. The difference in the nitrogen abundance using this C_β value is larger. The same is true for the neon abundance. Considering the very anomalous values of the log(Ne/O) ratio and the very low log(N/O) ratio obtained with the new set of line intensities, the Hγ/Hβ coefficient was used to derive the line intensities. To conclude, the difference in the abundances, between the regions A1/A2 and region D, cannot be an artifact of the reduction procedure.

Region D appears, in both the spectrum and the Hα image, as a two-component region, with a prominent stellar continuum at the southern part of the object. A possible explanation for the difference found in the metallicity could be the large distance, about 780 pc, of region D to the other four components of the galaxy, measured from the nearest edges of regions A1 and D. Moreover, this region seems not to be embedded in a diffuse envelope of gas surrounding the rest of the components (Heydari-Malayeri et al. 1990). These facts, in combination with the small difference in the radial velocity (200 km s^{-1}), indicate that this region does not belong to IC 4662. Instead it may be a compact, bright object residing slightly behind IC 4662, with two distinct regions of star formation. In order to test this hypothesis, detailed spectroscopy of all the four H II regions are needed to determine the velocity of each component in order to retrieve the dynamical state of the system. Other explanations for the difference in the abundances can also be invoked, such as galactic winds, dynamical disruptions, or a chemically poorly-mixed interstellar medium, due to its large distance from the other H II regions.

5.3. ESO 245-G05

As previously mentioned, it was not possible to use the Hα line in the extinction correction for both regions (see Sect. 4). One can ask how much this flaw will influence the final chemical abundances. A similar procedure to that described for region IC 4662 D was performed here.

For region nr. 19, a new set of line intensities was obtained corrected with the extinction coefficient obtained from the Hα/Hβ ratio. The total oxygen abundances obtained with this new set of data is very close to those presented in Table 6, with a difference of only 0.07 dex. For region nr. 12, a similar approach was taken, but no extinction coefficient could be obtained from the data using grism nr. 2, and a low value ($C_\beta = 0.03$) was found from the data using grism nr. 6. The latter value was preferred because no significant differences were found in the chemical abundances extracted.

Only the oxygen and neon abundances are compared in regions nr. 12 and nr. 19 in ESO 245-G05. This is due to the absence of the red spectral region for the latter region. For both elements, differences are found which is in agreement with the oxygen abundances obtained by Miller (1996). There is also a difference in the electron temperature, which could reflect a variation in oxygen abundance. The abundance variations could be a result of different star formation histories between regions nr. 12 and nr. 19. This was studied using Cerviño & Mas-Hesse (1994), where the age of the last star-forming event is obtained from the $T_{\rm ion}$ and the equivalent width of the Hβ emission line, $E_v(H\beta)$. The values of these parameters, extracted for region nr. 12, indicate an event younger than 3 Myr.

One of the many possible explanations for the difference in the chemical abundances could be that the last episode of star formation in this galaxy was initiated before the completion of the mixing of chemical elements.

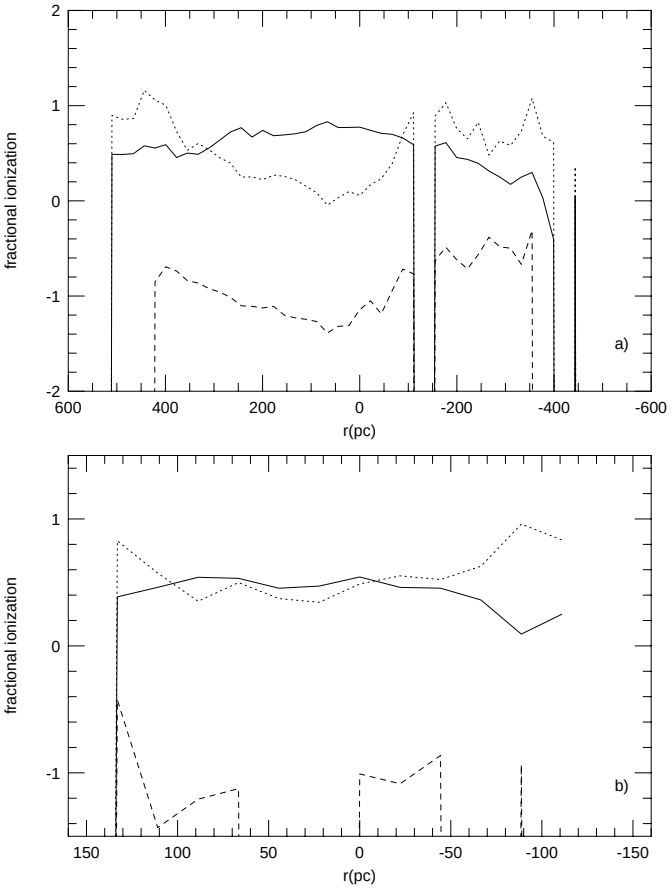

Fig. 4. The fractional ionization of the regions **a)** IC 4662 A1/A2 and **b)** IC 4662 D. The symbols have the following meaning; O^+/Hβ (— —), O^{++}/Hβ (——) and N^+/Hβ ($\cdots$)

6. Results on the spatial distribution in IC 4662

Due to the high quality of some of the data, a study of the excitation, the extension of the ionization zones and the spatial distribution in the chemical abundances within the H II regions A1/A2, and D in IC 4662, could be carried out. ESO 245-G05 will not be considered in this section due to the poorer quality of data.

6.1. The ionization structure in IC 4662

The ionization structure of the regions of IC 4662 is presented in Figs. 4a and b, corresponding to regions A1/A2 and D, respectively. The high ionization zone corresponds to physical positions of high [OIII]λ5007/[OII]λ3727 emission line ratios. Correspondingly, regions of low ionization region are those with high [OII]λ3727/[OIII]λ5007 line ratios.

From Fig. 4a, corresponding to the region IC 4662 A1/A2, it is evident that the high ionization region has an extension of about 400 pc, which agrees well with the extension of the excitation region (see the subsequent section). The low and high ionization zones are not so distinctive for region D (Fig. 4b), which indicate a relatively older age of the last episode of star formation. This agrees with the small equivalent width of Hβ (see Table 5).

6.2. The excitation structure of IC 4662

The excitation parameter, [OIII]λ5007/Hβ, for regions A1/A2 and D of IC 4662 is presented in Figs. 5a and b. Despite the results found by Heydari-Malayeri et al. (1990) regarding the existence of two distinct H II regions A1/A2, no such distinction is evident studying the excitation parameter (Fig. 5a). Instead, only one peak, extending almost 500 pc, is clearly visible while the Hα intensity is roughly constant throughout the entire region. The large spatial extension of the probable OB associations could indicate a situation more typical of a starburst phenomenon than that of a continuous star formation rate. This seems to be the case for dIs in general.

The excitation parameter seems to be largely constant in region D (Fig. 5b) although the Hα/Hβ ratio shows a minimum at 50 pc from the geometrical center of the H II region. This OB association is also extended, 200 pc, but the excitation is weaker than in region A1/A2. Comparing Fig. 5b with the Hα image of this galaxy, one sees two small concentrations which may correspond to the two peaks in the Hα/Hβ ratio. These peaks are also noticeable when studying the ionization structure (Fig. 4b).

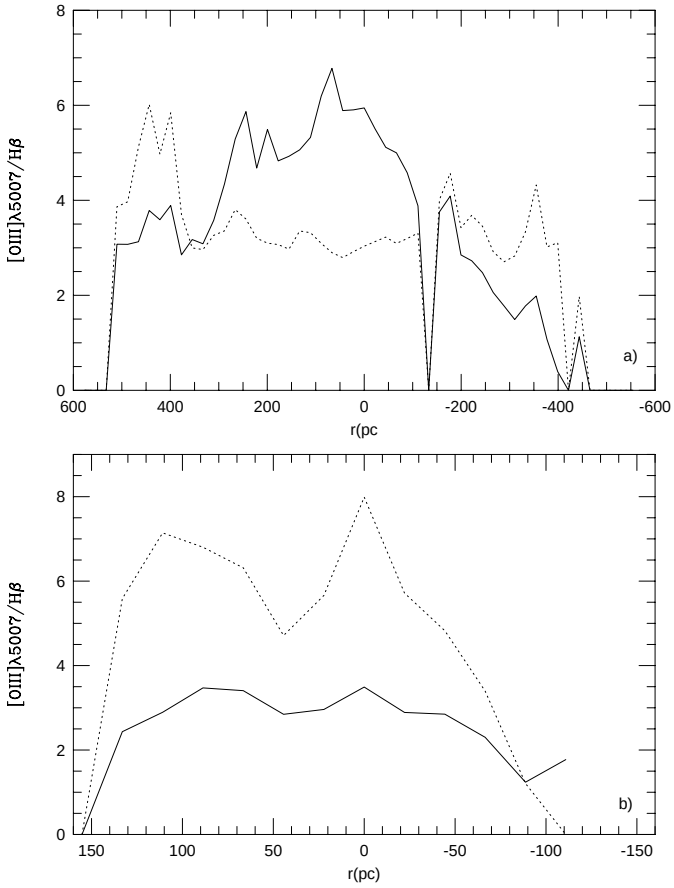

Fig. 5. The excitation parameter, defined as the emission line ratio [OIII]λ5007/Hβ (——), for **a)** IC 4662 A1/A2 and **b)** IC 4662 D. The non reddening-corrected Hα/Hβ ratio is also presented ($\cdots$)

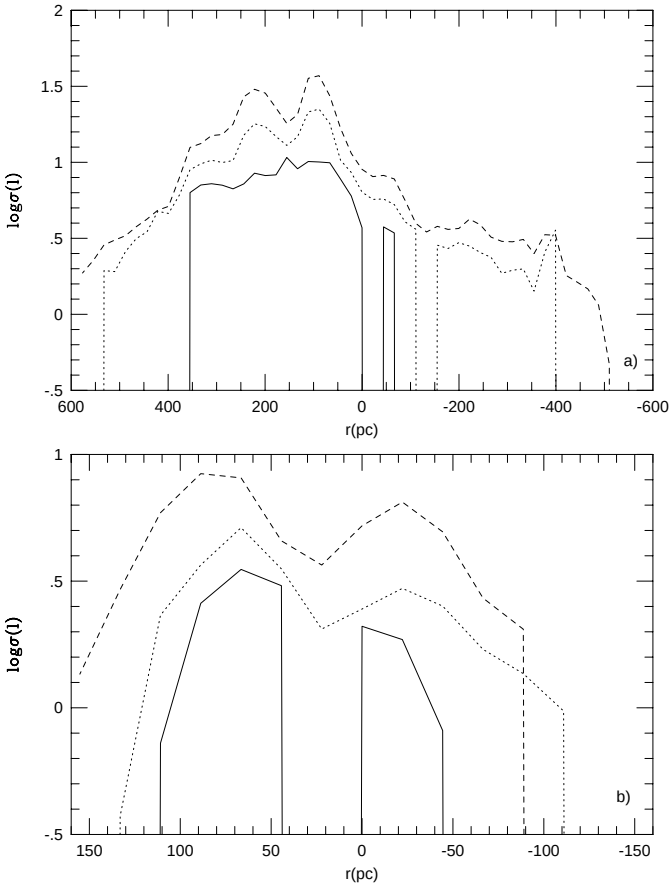

Fig. 6. The signal-to-noise ratio in the following three emission lines; [OIII]λ4363 Å(——), the Hβ ($\cdots$) and Hα (— —) is presented for **a)** IC 4662 A1/A2 and **b)** IC 4662 D

6.3. The distribution of chemical elements of IC 4662

Figures 6a and b present the spatial distribution of the signal-to-noise ratio determined from the 3r-spectra for regions A1/A2 and D. The signal-to-noise ratio differs by a factor of 10 in the most extreme case, comparing these H II regions. The signal-to-noise ratio of the [OIII]λ4363 Å line determined for regions A1/A2 (Fig. 6a) is considered to be sufficiently high for a reliable analysis, which is not the case for region D (Fig. 6b). It is concluded that the quality of the data of the latter is too poor for a study of possible variations in chemical abundances inside this H II region.

In the following, only the locations where the signal-to-noise ratio is higher than $\log(\sigma) = 0.9$, based on the Hα intensity, or $\log(\sigma) = 0.5$, based on the [OIII]λ4363 Å intensity, will be considered in the further analysis. The latter value is considered to be the lowest signal-to-noise ratio acceptable for a meaningful analysis (Rola & Pelat 1995).

6.3.1. Electron temperatures and oxygen abundances of IC 4662

The T_e over the face of A1/A2 in IC 4662 is presented in Fig. 7. The value obtained from the spatially-averaged spectra of the two regions is also visualized. One can note the largely uniform electron temperatures in the two regions.

An average T_e of 12 500 K was determined from the data of the 3r-spectra and agrees well with that from the spatially-averaged spectrum (12 000 K). The T_e seems constant throughout the regions but some deviations in this quantity seem to be evident, especially at 150, 20, 0, and -40 to -60 pc. From consulting Table 7 one can conclude that, considering the high signal-to-noise ratio in this region, no significant variations in the T_e are present. The variation in the T_e detected could be real or may reflect small-scale temperature fluctuations (Peimbert 1967) or possible variations in the ionization parameter, U. A more thorough study regarding these parameters is necessary in order to unveil the origin of the variations in the T_e. This is beyond the scope of this paper.

The oxygen abundance over the face of IC 4662 A1/A2, derived from the temperature-sensitive method (Osterbrock 1989), is presented in Fig. 8. Following Pagel (1997), a constant distribution of a chemical element is one where the differences found are smaller than 0.1 dex. Larger differences, which is the proper error of the method (Pagel 1997), will be considered real over/underabundances. With this definition, it is evident

Table 7. The maximum deviation in chemical abundances comparing the spatially-averaged spectra and the 3r-spectra for IC 4662 A1/A2. The first column is an order number; the spectrum denoted as number 1 corresponds to the first point to the left in Figs. 7 to 12 (although only rows 10 to 31 are used in the analysis). For the remaining columns, Δ is defined as $\Delta = (X_{\rm ave} - X_{\rm 3r})/(\Delta_{\rm ave} + \Delta_{\rm 3r})$, where $X_{\rm ave}$ is the value of the quantity derived from the spatially-average spectra and $\Delta_{\rm ave}$ the corresponding uncertainty. $X_{\rm 3r}$ and $\Delta_{\rm 3r}$ are the corresponding values of the 3r-spectra. Empty spacings mean that the values derived from the two methods coincide

3r-spectrum	ΔT	ΔO	ΔN	ΔNe	Δ(N/O)	Δ(Ne/O)
10	4900 K	0.45	0.43	0.18		0.19
11		0.18	0.09			0.17
12				0.09	0.05	0.03
13		0.03	0.1	0.04	0.13	
14						
15		0.06		0.06	0.22	
16						
17				0.02		0.04
18						
19	19	0.04				0.05
20	350 K	0.17	0.18	0.05		0.09
21			0.04			
22			0.05	0.01		
23						
24						
25		0.07				0.01
26		0.1	0.17			0.14
27		0.1	0.07	0.2		
29	650 K	0.1	0.1			
30		0.14	0.15			0.11
31		0.03	0.04	0.13		0.09

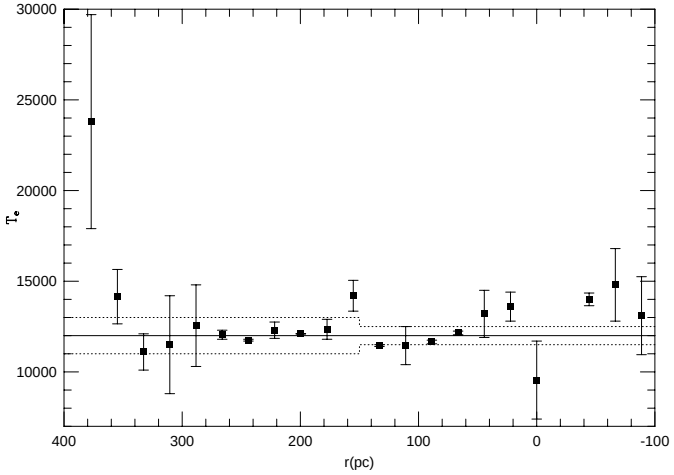

Fig. 7. The electron temperature, $T_{\rm e}$, of IC 4662 A1/A2. The value obtained from the spatially-averaged spectra of each region is also shown (——) with a 1σ deviation (— —). The spatially-averaged $T_{\rm e}$ is plotted only for the region of high signal-to-noise ratio. The H II region A1 is located between 150 and −100 pc, the region A2 between 400 and 150 pc

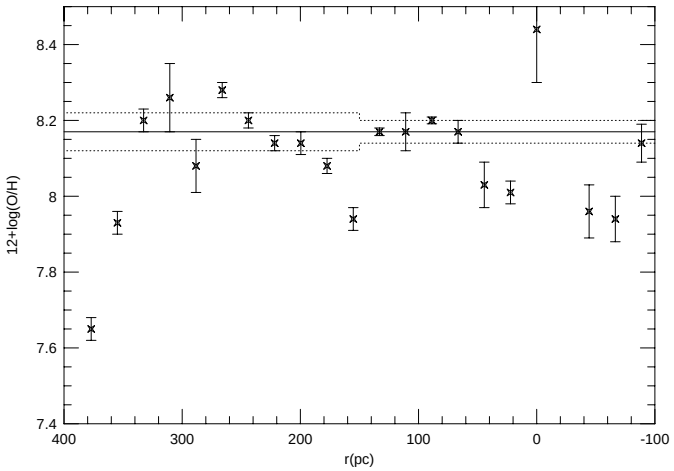

Fig. 8. The spatial distribution of (O/H) for IC 4662 A1/A2. The value obtained from the spatially-averaged spectra of each region is also shown (——) with a 1σ deviation (— —). The H II region A1 is located between 150 and −100 pc, the region A2 between 400 and 150 pc

that the oxygen abundance seems constant in region A1 (which corresponds to the rightmost part of the diagram) between 150 pc and 30 pc. However, important deviations from the average value are present in the spectra which could reflect a real underabundance in oxygen. The distribution of oxygen across region A2, between 400 and 150 pc, is more difficult to interpret.

It should be pointed out that the average oxygen abundance extracted from the 3r-spectra is slightly lower (8.10) than that derived from the spatially-averaged spectrum (8.17).

6.3.2. The distribution of helium, nitrogen and neon

By studying the distribution of helium it is obvious that the average value derived from the 3r-spectra (N(He)/N(H) = 0.10) is equal to the spatially-averaged helium abundance. Considering the high uncertainties associated with the helium abundance determination no conclusion regarding the possible variation of this element over the face of IC 4662 A1/A2 can be drawn.

The nitrogen distribution is presented in Fig. 9, (corresponding to spectra nr. 20, 26 and 29 in Table 7). A difference is found in the spatially-averaged abundances between regions A1/A2 (see Table 5). This is not particularly evident when the spatial distribution is studied. If restricted to the region of high signal-to-noise ratio only, the locations at 160, 20, and −40 pc (see Table 7) present a real difference in the abundance of nitrogen while a constant value can be inferred for the rest of the locations, considering the uncertainties involved. The nitrogen abundance determined from the 3r-spectra is slightly lower than that obtained from the spatially-averaged spectrum (0.13 dex).

Neon and oxygen are, mainly, the result of type II supernovae (SNe) explosions with stars more massive than ∼10 $M_\odot$ as progenitors. The abundance of these two elements should show a similar distribution and any spatial variations in oxygen should be mimiced by the distribution

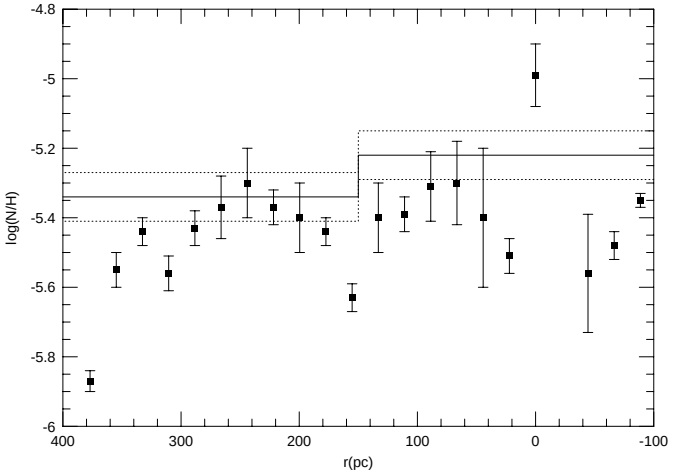

Fig. 9. The spatial distribution of log(N/H) in IC 4662 A1/A2. The value obtained from the spatially-averaged spectra of each region is also shown (——) with a 1σ deviation (— —). The H II region A1 is located between 150 to −100 pc, the region A2 between 400 to 150 pc

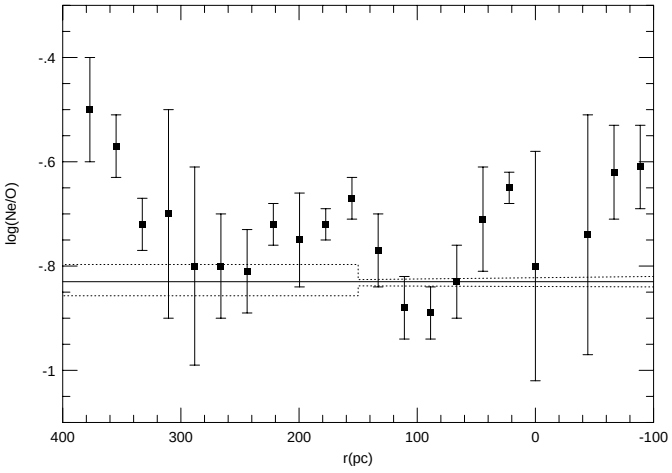

Fig. 11. The spatial distribution of log(Ne/O) in IC 4662 A1/A2. The value obtained from the spatially-averaged spectra of each region is also shown (——) with a 1σ deviation (— —). The H II region A1 is located between 150 and −100 pc, the region A2 between 400 and 150 pc

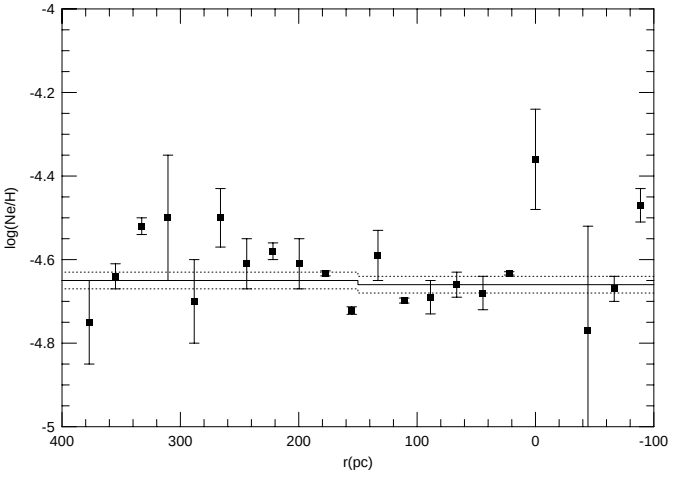

Fig. 10. The spatial distribution of log(Ne/H) in IC 4662 A1/A2. The value obtained from the spatially-averaged spectra of each region is also shown (——) with a 1σ deviation (— —). The H II region A1 is located between 150 and −100 pc, the region A2 between 400 and 150 pc

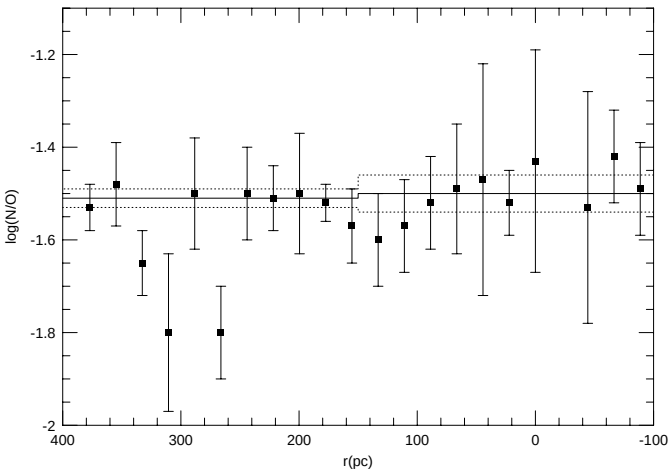

Fig. 12. The spatial distribution of log(N/O) in IC 4662 A1/A2. The value obtained from the spatially-averaged spectra of each region is also shown (——) with a 1σ deviation (— —). The H II region A1 is located between 150 and −100 pc, the region A2 between 400 and 150 pc

of neon. The distribution of neon is presented in Fig. 10 and should be compared with the distribution of oxygen (Fig. 8). Both elements show an overabundance at 0 and 266 pc (spectra nr. 15 and 27 in Table 7). The underabundance of oxygen at 44 and 22 pc (nr. 25 and 26 in Table 7) seems not to correlate with an underabundance in neon at those locations. It should be noted that the signal-to-noise ratios are comparatively high at these locations. Moreover, the location at 44 pc presents a normal, within the uncertainties, value of the ratio log (Ne/O), evident from Fig. 11. This is not the case at 22 pc, where the underabundance in oxygen seems to be real. The distribution of the ratio log (N/O) is presented in Figure 12. At most locations, this ratio is close to −1.5, which is typical for this kind of galaxies (Izotov et al. 1997), although underabundances in the log (N/O) ratio are evident between 260 and 310 pc.

The region around 0 pc (nr. 20 in Table 7) presents overabundances for all elements except nitrogen. One explanation can be the low signal-to-noise ratio in the emission line [OIII]λ4363 Å in this part of the spectrum. The region at 155 pc (nr. 27 in Table 7) reveals underabundances in all elements, and a possible explanation can be that this point marks the frontier between the two H II regions A1/A2. Another explanation for the abnormal values will be discussed in the next section.

7. Chemically homogeneous or non-homogeneous galaxies?

7.1. Small-scale variations

When small spatial scales are considered, the main conclusion from this investigation is that the abundances are nearly constant throughout the face of A1/A2 in IC 4662, except perhaps at a few locations. The spectral lines [FeII]λ4570 Å, HeIIλ4685 Å, and [ArIV]$\lambda\lambda$4711,4740 Å are clearly present at those locations where variations in some elements are found, as discussed in the previous section. In Sect. 5.2, it was concluded that the origin of the HeIIλ4686 Å line is not completely understood. If this line is due to WR stars or SN type II, the underabundance in helium at -22 pc can be explained as a result of sweeping of chemical elements by winds. Traces of chemical enrichment may be observed at the locations at -44 and 265 pc. A weak point in this argument is the non-symmetric distribution of the nebular edges, with the northeast very close by and the southwest further away. This could only be explained by a lower electron density ($N_{\rm e}$) in the interstellar medium along the northeast direction, as Recchi et al. (2000) have shown. Another problem is the size of the region where the possible WR spectral features are detected. The total size is 245 pc, which is almost one fifth of the total size of A1/A2. From the simulation performed by Recchi et al. (2000), the edge of the wave of an event of a SN explosion will travel a distance of nearly 1.5 kpc, given a luminosity of $L_{\rm b} = 1.5\ 10^{36}$ erg s^{-1}, where $L_{\rm b} = 17.9\ \rho_{\rm o}\ {H_{\rm eff}}^2\ {C_{\rm o}}^3$. $\rho_{\rm o}$ is the central density, $C_{\rm o}$ the speed of sound and $H_{\rm eff}$ the effective scale length of the ISM. Supposing that such a wave is detected in the data presented here, the distance from the event is only 125 pc (for a central event), and a $L_{\rm b}$ of $1.2\ 10^{35}$ erg s^{-1} is required, Using typical values of these quantities of 100 cm^{-3}, 4 km s^{-1} and 100 pc, respectively, a $L_{\rm b}$ of $1.14\ 10^{39}$ erg s^{-1} is obtained, which is higher than that required. In principle, two SN events could be the explanation for the "double-bowl shape" of the distribution of those elements, from 300 to 0 pc; one at 22 pc, the other at 155 pc. The helium abundance was found to be largely constant throughout the H II regions. It should be emphasized that the contribution of singly-ionized helium was not considered in the derivation of the total abundances.

A final point concerning the helium and nitrogen distribution is the expected enrichment of these elements when the WR/SN features are observed. As mentioned, no significant enhancement of helium is found in the locations where the HeIIλ4686 Å line is detected and the abundance of nitrogen is constant in the same locations or, perhaps, somewhat depleted. The results presented here are consistent with the suggestion that helium and nitrogen emerging from the present epoch of star formation are only detectable in X-rays due the high temperatures involved (Kobulnicky et al. 1997).

7.2. Large scale variations in chemical abundances

The discussion of possible inhomogeneities in chemical abundances of the ISM within dwarf galaxies has been considered for many years. Part of the data support the idea of a homogeneous chemical composition which is in line with a closed-box model (Tinsley 1980). This model seems to behave well for giant, dynamically stable elliptical galaxies. The situation for dwarf galaxies may be different because of their small gravitational potentials, which could make the galaxy partially unstable to strong interstellar winds or external gravitational influences. Selective loss of chemical elements through winds has been proposed in order to explain the chemical abundances observed in dwarf galaxies (Pilyugin 1992; Matteucci & Tosi 1985). The situation is unclear since the results of the modeling vary from those where chemically enriched gas remain in the galaxy, to those where the metals are partially ejected from the galaxy in a selective manner (D'Ercole & Brighenti 1999).

The typical model of chemical evolution for dwarf irregular galaxies contains self-enrichment (total or partial) of the ISM due to previous events of star formation. These events are spaced out to a few Gyr. During the quiescent phases, elements ejected will cool until reaching the temperature of the ISM and is assumed to mix with the rest of the ISM. The mixing is supposed to be homogeneous and efficient throughout the galaxy by any of the mixing processes proposed: e.g., epicyclic or radial mixing, superbubble expansion (Roy & Kunth 1995). These processes would erase any abundance variations on timescales less than 10^9 years. Under such circumstances, a new event of star formation can occur when the mixing of elements is completed and the chemical composition throughout the ISM would remain the same. I Zw 18 (Izotov et al. 1999) and NGC 4214 (Kobulnicky & Skillman 1996) seem to be good examples of chemically homogeneous galaxies. However, a few other galaxies do not show a homogeneous chemical composition, e.g. WLM (Hodge & Miller 1995) or IC 10 (Lequeux et al. 1979)

Three dI galaxies have been studied in this series of articles in order to increase our knowledge of this subject. As is evident, no unique answer to whether dIs are homogeneous or not has been obtained. It seems logical that the mechanisms acting in favour of mixing the ISM does not work with the same efficiency in all cases. Actually, some of the mechanics more efficient in the mixing are believed not to be operating in dwarf galaxies. This could simply be a consequence of the physical conditions and morphology of each particular galaxy, or region of a galaxy. Each of the three dIs studied, the two presented in this article and NGC 6822 (Paper I) should be considered independently.

The study of NGC 6822 (Paper I) showed almost no variations in chemical composition between the H II regions, while for the other two, IC 4662 and ESO 245-G05, some deviations are found. As discussed in Paper I, the two H II regions of NGC 6822, Hubble V and Hubble X, are situated in the northern part of the bar. The small

distance between the H II regions probably acts in favour of the minor variations in the chemical abundances.

ESO 245-G05 is an exceptional case. All the H II complexes except one, which include regions nr. 5, 6 and 7 in Miller (1996), are located along the bar of the galaxy. It is well known that, as the ellipticity of a bar increases, the smaller the difference in the abundances (Martin & Roy 1994). External gravitational interactions could play a role. A number of explanations could be proposed for the variations in the abundances, e.g. shorter events of star formation, which would act to inhibit complete mixing of the elements. This would especially be the case for large galaxies such as ESO 245-G05. Infall of primordial gas or interaction with HI clouds could be the main processes triggering star formation before the completion of the mixing of the elements. If continuous star formation is invoked for this kind of galaxy (Legrand 1999), the explanation is more reasonable since the mixing timescale would be longer.

IC 4662 is the most striking galaxy in this sample. As a result of the morphology (small, non-barred galaxy), its physical environment (isolated) and the fact that IC 4662 is dominated by a powerful event of star formation, a homogeneous distribution in chemical abundance would be expected for this galaxy. In agreement with this, no differences have been found between the H II regions A1/A2. The chemical homogeneity of A1/A2 could be a consequence of the proximity of the regions. Actually, no clear distinction between these regions could be found studying two-dimensional spectra and one should perhaps regard A1/A2 as a single H II region. However, region D shows completely different chemical abundances, compared to A1/A2, for all elements studied.

The large distance between region D and the main body of the galaxy, and the fact that this region seems to be located outside the HI cloud (Heydari-Malayeri et al. 1990), could be the explanation for the different chemical abundances. The homogenization mechanisms which work at large scales are less efficient for dIs due to longer timescales for the mixing of the gas. For the rest of the galaxies with high quality spectra, no inhomogeneities have been detected, except for NGC 5253 (Kobulnicky et al. 1997). Some of these galaxies are larger than 1 kpc, e.g. NGC 4214, which exceeds the distance between region D and the rest of the regions. However, in all these cases there seems to be a dynamical connection between all the H II regions studied, which is not the case for IC 4662.

Finally, two galaxies in this investigation (NGC 6822 and ESO 245-G05) have gravitational companions (consult Hidalgo-Gámez & Olofsson 1998 for their definition of gravitational companion), which could affect the star formation history, as well as the gaseous mixing processes. The largest galaxy in the sample is ESO 245-G05 and the smallest is NGC 6822. The results presented in this investigation support the idea that the larger the galaxy, the more inhomogeneous its chemical composition. Moreover, the H II region which presents the largest differences in chemical composition in IC 4662 is A1/A2, which is the one most distant from the main body of the galaxy.

8. Conclusions

A detailed analysis regarding chemical abundances of three galaxies have been carried out in this series of articles. For two of the galaxies, NGC 6822 studied in Paper I and IC 4662, the quality of spectra were sufficiently high for an analysis of the spatial distribution of some important parameters. The main results concerning the spatial distribution for these objects are: the H II region in IC 4662 A1/A2 may be experiencing SN explosions or powerful WR stellar winds. This could be the reason for the differences found in the distribution the chemical elements across the face of the object.

An investigation regarding chemical abundances between different H II regions gave the following results. NGC 6822 shows no significant difference in the abundances between the two regions Hubble V and Hubble X, while important variations in all elements were found in IC 4662 and ESO 245-G05.

Acknowledgements. The authors want to thanks Prof. J.-R. Roy for many useful comments which improved the quality of this paper. Dr. P. Leisy is thanked for his assistance during and after the observations. M. A. Pharasyn is acknowledged for his help with part of the software used in this investigation. Dr. N. Bergvall is thanked for supplying and updating a new version of his software. An anonymous referee is acknowledged for valuable comments, suggestions and clarifications. A. M. H. G. has been financially supported by NOTSA and by UAO. A. M. H. G. thanks the Instituto de Astrofísica de Andalucía for their hospitality and to Dr L. Binette for financial support by the CONACyT grant 32139-E.

References

Aller, L. H. 1984, Physics of gaseous nebulae (Reidel Publishing Co., Dordrecht)
Becker, R., Mebold, U., Reif, K., & van Woeder, H. 1988, A&A, 203, 21
Cerviño, M., & Mas-Hesse, J. M. 1994, A&A, 284, 749
D'Ercole, A., & Brighenti, F. 1999, MNRAS, 309, 941
Fillipenko, A. V. 1982, PASP, 94, 715
González-Delgado, R. M., Pérez, E., Tenorio-Tagle, G., et al. 1994, ApJ, 437, 239
Harnett, J. I. 1987, MNRAS, 227, 887
Heydari-Malayeri, M., Melnick, J., & Martin, J.-M. 1990, A&A, 234, 99
Hidalgo-Gámez, A. M., & Olofsson, K. 1998, A&A, 334, 45
Hidalgo-Gámez, A. M., Olofsson, K., & Masegosa, J. 2001, A&A, 367, 388 (Paper I)
Izotov, Y. I., Thuan, T. X., & Lipovetsky, V. A. 1997, ApJS, 108, 1
Izotov, Y. I., & Thuan, T. X. 1999, ApJ, 511, 639
Kobulnicky, H. A., Skillman, E. D., Roy, J.-R., Walsh, J. R., & Rosa, M. R. 1997, ApJ, 477, 679
Kobulnicky, H. A., & Skillman, E. D. 1996, ApJ, 471, 211
Lequeux, J., Rayo, J. F., Serrano, A., Peimbert, M., & Torres-Peimbert, S. 1979, A&A, 80, 155

Legrand, F. 1999, Ph.D. Thesis
Martin, P., & Roy, J.-R. 1994, ApJ, 424, 599
Matteucci, F., & Tosi, M. 1985, MNRAS, 217, 391
McCall, M. L., Rybski, P. M., & Shields, G. A. 1985, ApJS, 57, 1
McGaugh, S. S. 1994, ApJ, 426, 135
Miller, B. W. 1996, AJ, 112, 991
Olofsson, K. 1997, A&A, 321, 29
Osterbrock, D. E. 1989, Astrophysics of gaseous nebulae and active galactic nuclei, University Science Books, Mill Valley, CA
Peimbert, M. 1967, ApJ, 150, 825
Pilyugin, L. S. 1993, A&A, 277, 42
Recchi, S., Matteucci, F., D'Ercole, A. [astro-ph/0002371]
Rola, C., & Pelat, D. 1994, A&A, 287, 676
Rosa, M., Joubert, M., & Benvenuti, P. 1984, A&A, 57, 361
Roy, J.-R., & Kunth, D. 1995, ApJ, 294, 432
Sanders, D. B., Egami, E., Lipani, S., Mirabel, I. F., & Soifer, B. T. 1995, AJ, 110, 1993
Savage, B. D., & Mathis, J. S. 1979, ARA&A, 17, 73
Stasińska, G. 1990, A&AS, 83, 501
Tinsley, B. 1978, Fund. Cosm. Phys., 5, 287
Trinchieri, G., Fabbiano, G., & Bandeira, R. 1989, ApJ, 342, 759
de Vaucouleurs, G. 1975, Galaxies and the Universe, ed. Sandage (The University of Chicago Press), 557
de Vaucouleurs, G., de Vaucouleurs, A., Corwin, H. G., et al. 1991, Third Reference Catalogue of Bright Galaxies (ed. Springer-Verlag)